Journal of Materials Chemistry A

Accepted Manuscript

ROYAL SOCIETY OF CHEMISTRY

www.rsc.org/materialsA

Template-free Synthesis of Boron Nitride Foam-like Porous Monoliths and Their High-end Applications in Water Purification

Yanming Xue[#,†,*], Pengcheng Dai[#,ǂ,*], Xiangfen Jiang[†], Xuebin Wang[†], Chao Zhang[†,ǂ], Daiming Tang[†], Qunhong Weng[†], Xi Wang[†], Amir Pakdel[†], Chengchun Tang[‖,⊥,*], Yoshio Bando[†] and Dmitri Golberg[†,ǂ,*]

[†]*International Center for Materials Nanoarchitectonics (MANA), National Institute for Materials Science (NIMS), Namiki 1, Tsukuba, Ibaraki 3050044, Japan*
[ǂ]*Research Institute of Unconventional Petroleum and Renewable Energy, China University of Petroleum (East China), Qingdao 266580, P.R. China*
[‖]*School of Materials Science and Engineering, Hebei University of Technology, Tianjin, 300130, P.R. China*
[⊥]*Hebei Key Laboratory of Boron Nitride Micro- and Nano-Materials, Tianjin 300130, P.R. China*
[ǂ]*University of Tsukuba, Tennodai 1, Tsukuba, Ibaraki 3050005, Japan*
[#]*These authors contributed equally to this work.*

[*]*E-mail:*
XUE.Yanming@nims.go.jp
dpcapple@upc.edu.cn
tangcc@hebut.edu.cn
golberg.dmitri@nims.go.jp

Keywords: template-free synthesis, boron nitride, porous monoliths, water purification

Abstract:

It has remained a great difficulty and challenge to prepare BN-based porous monoliths (BNPMs) via a facile method. Here, we report a brand-new and high-throughput synthesis of BNPMs through a facile two-step template-free reaction including self-bubbling precursor solidification and high-temperature pyrolysis. The resulting BNPMs with an interconnected open-bubble structure exhibit the highest specific surface area ever reported for the BNPM systems, up to 1406 m^2/g, and high bulk crush strength of ~ 1 MPa. Thanks to their spacious hydrophobic surfaces, the material was applied for the high-efficient separation-adsorption purification of an oil/water system, demonstrating an excellent adsorption capacity of up to 71% - 98% (volume-based adsorption capacity) toward a wide selection of oil contaminants. Besides, the present BNPMs were designed as a filtration column which rapidly removes rhodamine B (RB) and Cd(II) pollutants from an aqueous solution under a forced filtration-adsorption process, corresponding to the ultrahigh removal capacity of 554 mg/g and 561 mg/g, respectively. Thus, the obtained BNPMs are envisaged to become a fairly promising adsorbent for water cleaning.

Introduction

Porous monolith materials (PMMs) have attracted much interest, particularly in regards of separation-purification/-adsorption applications due to their diverse porous structures.[1-4] Currently, PMMs are made of carbon (C) and silica (SiO_2),[5, 6] however which suffer from their poor chemical and thermal stabilities in regeneration. Among other light-weight alternatives, boron nitride (BN) is famous for its distinguished chemical inertness and excellent oxidation resistance. Thus it has seriously been considered as a promising candidate for PMMs.[7, 8] On the other hand, to date, the exploitation and utilization of BN-based porous monoliths (BNPMs) have remained hardly available due to synthetic difficulties and limitations of successful fabrication methods discovered. BNPMs have been developed via a complex template-assisted approach by Miele et al.[9-11] Their methods used porous silica as a template to fabricate porous carbon, and the as-obtained porous carbon then acted as a template for the BNPM synthesis. Such two-step template-assistant route is lavish and further needs the usage of toxic chemicals, such as HF to remove the template, while the precursors for BN formation are borazinic species, which are poisoned, unstable and quite expensive. In addition, the final BNPM formings were subjected to a spark plasma sintering (SPS) under a temperature up to 1700 °C[9, 10] or a thermal treatment performed in ammonia at 1000 – 1450 °C[11]. Taking energy conservation and environment protection into consideration, these methods are not advantageous for a large-scale BNPM production. Factually, the lack of large quantity production of BNPMs restrains their application studies and smart technological designs. Therefore, seeking a simple, energy-saving and high-yield methodology that enables practical development and application of BNPMs is a timely-warrant task.

Currently, many investigations have demonstrated that BN-related porous powder adsorbents show advantageous applications compared to many conventional adsorbents in separation, adsorption and purification ranging from organic pollutants to gases. This is because they possess many specific features, such as peculiar B-N bond polarity, distinct chemical inertness, an ultrahigh specific surface area (SSA) and adsorption capacity.[12-18] However, to our best knowledge, the studies of BNPMs in such applications have not been yet performed.

Here, we demonstrate a simple template-free method for constructing a foam-like BNPM with high SSA, up to 1406 m^2/g, and decent bearable compressive stress of 1 MPa. The typical synthesis included a two-step process for controlling self-bubbling solidification of boric acid-dissolved formaldehyde-dicyandiamide resin, and high-temperature pyrolysis reaction with ammonia within a relatively moderate temperature range of 1000 – 1200 °C. In comparison with the previous fabrication procedures mentioned above, no template was used by us during the preparation, and the formaldehyde-dicyanodiamide resin, boric acid and ammonia used are all cheap and non-toxic. This approach would lead to a facile and high-throughput fabrication of BNPMs. In addition, for the first time, the obtained BNPMs were effectively employed for oil adsorption; they showed an excellent sorption performance for a wide range of oil species. Having good oxidation resistance and notable chemical inertness they easily recovered and exhibited excellent recycling stability. Finally we document that BNPMs may nicely work as a filtration column for toxic organic dye rhodamine B (RB) and heavy metal ion Cd(II) under a suction filtration process.

Experimental Section

All chemical reagents were of commercially analytic grade, available from Wako Pure Chemical Industy, Co. Ltd, and used as received without further purification.

Synthesis of BNPMs: (1) Preparation of formaldehyde-dicyanodiamide resin (FDR): firstly, 8.4 g dicyanodiamide (0.1 mol) was dissolved into 5 ml formaldehyde solution (37% by weight) in a 250 ml three-neck round-bottom flask which was connected with a water condenser tube onto its one neck, then vigorous stirring in an oil-bath at 85 °C was performed, to obtain a transparent mixture liquid; secondly, the transparent liquid was continuously reacted at these conditions (stirring at 85 °C) for at least 1 h, to form a transparent FDR solution. (2) Preparation of boric acid-dissolved formaldehyde-dicyanodiamide resin (BAFDR): firstly, 4.2 g boric acid (H_3BO_3, ~ 0.068 mol) was dissolved into the FDR under continuous stirring in an oil-bath at 85 °C, to form a transparent and viscous mixture liquid; secondly, the mixture was continuously reacted at 85 °C under stirring for at least 1 hs to obtain the transparent and viscous BAFDR liquid. (3) Fabrication of BNPMs: firstly, the BAFDR liquid was transferred into a slender cylindrical container tightly coated with a stopper with a very small hole in it; secondly, the container was heated in a drying oven at 180 °C for 12 h to achieve a self-bubbling solidification (during this solidification process, it must be ensured that the stopper was always tightly plugged into the container mouth in order to limit the self-foaming curing process occurring in this closed space to form a columnar bulk; gases generated in this process were completely released through the small hole in the stopper,) and obtain the monolithic columnar precursor, in addition, the BAFDR liquid was also extruded from the container along the small hole to form puffed-rice-rod-like monolithic precursors having the same monolithic structures as those inside the container (see Supporting Information (SI) Figure S1); finally, the BNPMs were obtained by pyrolyzing the solidified monolithic precursors above 1000 °C in an ammonia atmosphere for 6

h using a heating rate of 5 °C/min and an ammonia flow rate of 200 mL/min. The samples obtained at 1000 °C, 1100 °C and 1200 °C were notated as BNPM-1000, BNPM-1100 and BNPM-1200, respectively.

Oil adsorption experiments: To investigate the adsorption capacities for oil classes, the weight-known BNPM-1100 samples were placed into the oil solvent (see SI Video SV2). After adsorption was finished, the BNPMs were removed from the oil, and weighed again when the wet monoliths had been drained without any residual oil droplet. The adsorption capacity (C_a) was calculated using $C_a = \frac{M_t - M_0}{M_0}$ equation (where M_t and M_0 are the weights of BNPMs after and before the oil adsorption, respectively).

Filtration adsorption experiments: The filtration experiments for RB and Cd(II) adsorption were performed employing a stuffing BNPM-1100 column (50 mg) placed into a U-type glass tube with inner diameter of ~ 0.7 cm (a sand-core filter column was tightly plug into the bottleneck zone of the tube, and BNPM column was tightly compacted onto the sand-core filter column); and then either RB or Cd(II) solutions were automatically pumped through the BNPM filtration column; finally the filtered water was collected in a collection bottle connected with the other end of U-type glass tube, as shown in SI Figure. S9 and Video SV2. The concentration of RB aqueous and alcoholic solutions before and after filtration adsorption and desorption was determined by detecting their maximum intensities of photoluminescence (PL) emission peaks (using a Fluorescence Spectrophotometer, HATACHI F-7000) and UV-Vis absorption spectra (UV-Vis-NIR Spectrometer V-570). The Cd(II) filtration adsorption was conducted by using the same method. The concentration of Cd(II) aqueous solution before and after the filtration adsorption was determined by using ICP measurements (ICP Optical Emission Spectrometer, SPS3520UV).

Estimate of the ion-exchange capacity: Firstly, a BNPM-1100 powder (50 mg) was immersed into 60 mL 0.2 M HCl solution under a powerful stirring for 24 hs, and then the powder adsorbent was washed with a deionized water repeatedly (at least 10 times) to remove traces of acid; secondly, the BNPM-1100 powder after acidizing was immersed into the equilibration solution (deionized water) for 6 hs, after this equilibration the powder adsorbents were then immersed into 30 mL of 0.03 M NaOH solution for 24 hs; thirdly, 0.03 M HCl was used to titrate the moles of NaOH after equilibration. The cation-exchanged capacity of BNPM-1100 powder was determined by using the following Equation (1):

$$C_{ie} = (M_0\text{-}M)/m \quad (1)$$

Where C_{ie} is the capacity of ion exchange, the M_0 is the moles of 0.03 M NaOH solution before equilibration, the M is the moles of the NaOH solution after equilibration, and *m* is the mass of the as-used BNPM-1100 powder.

Characterizations: XRD data of the samples were collected using a Rigaku Ultima III (Cu Kα radiation) diffractometer; the morphology and structure analyses were performed by SEM (Hitachi S-4800, at the accelerating voltage of 5kV, and with scanning speed of 5 °/min), HRTEM (JEM-3000f, and JEOL JEM-3100FEF, with accelerating voltage of 200kv) equipped with an energy loss spectrometer (EELS); the chemical compositions and bond characters were characterized by X-ray photoelectron spectroscopy (XPS, JPS-9010TR, JEOL, with an Mg Kα X-ray source) and FT-IR (Thermo Nicolet 4700, with pure KBr as the background, wave-number range of 4000-400 cm^{-1} and standard resolution of 0.4 cm^{-1}); the bulk crush strength was conducted by using a tension test machine (SHIMADZU EZ-S, Japan, with maximum loading pressure of 50 N); the zeta potential was measured on an electric and particle analyzer (ELSZ-2000ZS) at room temperature, the as-measured turbid liquid was the ground BNPM-powder

solution with different pH value; the N_2 adsorption-desorption isotherms were obtained by using an automated gas sorption instrument (Quantachrome Autosorb-IQ2 SYSTEM) at 77 K; the contact angle measurements were performed using an automated digital goniometer (DropMaster DM-701, KYOWA), a deionized water droplet of about 10 μL volume, and a high-resolution Keyence VH-5000 optical instrument. The thermostability analysis was done using thermogravimetry (TG) and differential thermal analysis (DTA) methods (Rigaku Thermo Plus TG 8120) with thermal ration of 10 °C/min in air flow.

Results and discussion

The synthesis process of BNPMs is schematically sketched in Figure 1. A transparent viscous precursor liquid (BAFDR) was prepared via a reaction of formaldehyde solution, dicyanodiamide and boric acid in a reflux device with oil bath at 85 °C. A transformation from the liquid to a monolithic solid was accomplished under FDR polymerizating at 180 °C. Due to the uniform self-bubbling emerged during the solidification, the obtained monolith precursor possessed a much more inflated volume than the original liquid, and transformed into a foam-like 3D architecture structure. A uniform pyrolysis process was carried out in the ammonia atmosphere above 1000 °C, thus realizing a facile one-step convertion from precursor monoliths to the BNPMs, which is more convenient procedure than those described in the previous works[9-11] usually were complicated and required high-temperature pyrolysis, template removal, and even sintering processing and/or thermal treatments.

As presented in Figure 2a, the monolithic precursor is well shaped and crack-free. After the pyrolysis reaction with ammonia at 1100 °C, a BN product (BNPM-1100) keeps the unchanged monolithic shape, but reveals a distinct shrinkage of 66% in volume and ~ 30% in linear dimensions (e.g. 32% and 35% in longitudinal and radial directions, respectively). This

indicates that the original monolithic precursor has a homogeneous composition and consists of B, N, C and O species, and undergoes a homogeneous pyrolysis toward BN. The precursor had an amorphous structure with no obvious sharp crystalline peaks but only one broad band (ranging from 15° to 25°) as seen in the XRD pattern (Figure 2b). For the BNPM-1100 sample, a *d* value of (002) plane is ~ 0.37 nm, which is far larger than the (002) interplanar distance in well-crystallized h-BN (~ 0.33 nm)[19]. Thus, the present ordering type in BNPM-1100 should be assigned to the well-known turbostratic BN (t-BN) structure[20] (SI Figure S2). SEM examinations revealed that the BNPM had been composed of open-hole porous structures (Figure 2c-e) interconnected and strutted with the self-supported bubble walls (Figure 2e and 2f), which are created under gas-bubbling during solidification process. It is considered that the FDR-polycondensation process was accompanied by a large amount of heat produced. Such condensation polymerization triggered a drastic evaporation of water in the liquid, and induced the excess dicyandiamide to decompose into gas phases, such as NH_3 and HCN[21], leading to gas-bubbling during the BAFDR solidification. The bubbles' diameter and their wall thickness distributions are peaked at ~ 13 μm and ~ 2.7 μm, corresponding to the average values of ~19 μm and 3 μm, respectively (Figure 2g and 2h). Moreover, some macropores (with diameter of ~ 1 μm) were embedded in the bubble wall, as shown in the yellow frame of Figure 2f. From SEM images, we can see that the skeleton of the BN monolith consists of interconnected bubble walls, which create abundant megapores in the BNPM framework.

TEM analyses indicate that there are many micropores randomly distributed in the framework, as shown in Figure 3. As shown in Figure 3a, TEM images illustrate that the BNPM matrix is homogeneous in composition without any detectable mesopore (Figure 3a). A high porosity of the structures is particularly revealed by HRTEM characterizations on the BNPM

bulk edges (Figure 3b and c). Such BNPM possesses many visible pores randomly distributed within the t-BN layer networks (Figure 3b). The labeled locations (framed as A in Figure 3c) show the possible structural models constructed using unparallel and crossed (or nearly orthogonal) (002) layers, which result in high porosity. There are two types of pores (marked as P1 and P2 regions in Figure 3c) clearly observed under HRTEM. One (P1) is formed by unparallel or/and looped BN (002) layers, corresponding to the notably enlarged spacing between stacked (002) planes. The pore appearance is similar to that of the highly porous BN microsponges previously reported by our group.[22] The other (P2) is the interlaced combination of diversified defect structures, including the helical screw, radical-rich edge, and Y-form dislocations[17]. The average distance between parallel adjacent (002) fringes (C region in Figure 3c) is 0.367 nm, which matches well with that derived from XRD data. The distance between the two neighboring bright spots (B region in Figure 3c) is 0.258 nm (Figure 3d), perfectly corresponding to N-N or B-B atom separations in h-BN (002) planes.[23] This value indicates that some (002) layers in this t-BN phase presume a well-ordered B and N-alternanting hexagonal pattern. It is considered that the high-temperature pyrolysis with ammonia could efficiently remove the FDR-introduced C element (along with the reaction: $C + NH_3 \rightarrow CH_4 + N_2$).[17, 24] In addition, offsetting the loss of N source due to a decomposition of the solidified BAFDR-based precursor, the introduced ammonia would preferably favor the complete conversion of B-O into B-N at high temperature ($\geq$ 1000 °C) [17]. Due to a fact that the pre-formed B-N-B bonds (their existence was confirmed by FTIR data in SI Figure S3) worked as a primary BN-based framework in the homogeneous precursor, both the removal and conversion would leave pores and defects in the original C and O positions, enabling the monolith to possess a rich porosity after the pyrolysis.

We investigated the SSAs and porosity of the BNPM-1000, BNPM-1100 and BNPM-1200 via N_2 adsorption-desorption isotherms at 77 K (Figure 4a). All the adsorption-desorption isotherms are of type I, indicating typically dominated microporous characteristics.[25] The adsorption drastically increases in a low relative pressure (P/P_0) range, and without obvious hysteresis loops.[25] The as-selected P/P_0 range for standard Brunauer-Emmett-Teller (BET) analyses is confined within 0.025 - 0.28 (SI Figure S4). The SSAs of BNPMs increase from 1149 to 1406 m^2/g when the synthesis temperature changes from 1000 to 1100 °C, which is the largest SSA value reported to date for the BNPM materials (the highest SSA values are 428 and 299 m^2/g, respectively, for the BN monoliths obtained by porous BN powder-based SPS processing[9,10] and template-assisted integrative chemistry[11]). Temperature rising to 1200 °C and holding for 6hs makes the corresponding SSA to decrease (to 847 m^2/g). The SSA shrinkage is attributed to the ordering or crystallization of the t-BN phases within BNPM at 1200 °C (SI Figure S2). Their cumulative total pore volumes (at $P/P_0 = 0.997$) exhibit a similar first increased and then decreased trend, in a raw: 0.680 cm^3/g (at 1000 °C), 0.887 cm^3/g (1100 °C) and 0.485 cm^3/g (1200 °C). Quenched solid density functional theory (QSDFT) was employed to calculate and analyze the pore-size distributions (PSDs). This method takes into account the effects of surface inhomogeneity and roughness on geometrically and chemically disordered micro- and meso-porous structures [26, 27] which is applicable in the case of the present turbostratic/disordered BNPMs. The calculation reveals well-matched fitting with the experimental isotherms (SI Figure S5). The PSDs display almost the same characteristic pore sizes, i.e dominating sharp peak at ~ 0.9 nm, and the broad bands from ~ 1.2 to ~ 3.0 nm (centered at ~ 1.9 nm), as shown in Figure 4b. All BNPM samples have micropore volume ratios up to ~ 60% of the total volume (SI Table S1). Based on the N_2 sorption analysis, and SEM and TEM results, the obtained BNPMs were

determined to exhibit hierarchical porous structures including megapores, macropores and micropores.

The chemical composition of BNPM-1100 was characterized by spatially-resolved elemental mapping using EELS, Figure 5a-f. The segregation distributions for individual B, N, C and O elements reveal a major composition of B and N together with a minor C and marginal O contents. The overlay/separation maps reveal that each element exhibits uniform distribution. The distinct B K-edge (~ 190 eV) and N K-edge (~ 401 eV) with sharp π^* and σ^* bands in the resultant EEL spectrum illustrate well-hybridized sp^2 bonding in the BNPM (Figure 6a).[28] Furthermore, XPS measurements on the B1s and N1s signals (Figure 6b and c) present B1s and N1s peaks located at 190.3 eV and 398.0 eV, respectively.[29-31] Both B1s and N1s spectra imply that the B-N bonds exist in BNPM, this identical to the standard hexagonal BN.[29-31] The chemical composition analysis demonstrates that the B/N ratio of BNPM-1100 is ~ 1/1, the B+N sum is up to 95 at %; C (0.1 at.%) and O (< 5 at.%) contents are marginal (SI Table S2). In addition, the shoulder peaks fitted at 192.4 eV and 399.8 eV are attributed to –OH and $–NH_2$ groups attached on the surfaces,[32, 33] which correspond to the FTIR characteristics of –OH and $–NH_2$ groups (SI Figure S3). The well-stabilized –OH and $–NH_2$ groups imply chemical activity of BNPMs, as reported previously[14]. It is notable that these active groups have no effect on the innate hydrophobic nature of BN (SI Figure S6): the BNPM-1100 exhibited a water contact angle of ~ 146° and could float on an aqueous solution without water infiltration for at least 2 days.

The representative BNPM-1100 can be conveniently utilized to rapidly adsorb oil from the water surface (Figure 7a-c and SI Video SV1). This BNPM exhibited stable adsorption performance over 5 recoveries by burning oil-saturated matter in air (Figure 7d) followed by

annealing in ammonia atmosphere at 900 °C without changing a bulky monolith shape (SI Figure S7). The adsorbent can still adsorb a mass of salad oil up to ~ 5 times of its original weight, and the oil-saturated BNPM-1100 can still float on the cleaned water surface, and is easily clipped off. It is noteworthy that the 5-cycle recovered BNPMs not only have any damage of their monolithic shapes but also keep a decent overall compressive strength to preserve their monolithic microstructures (Figure 7e, primitive one with ~ 1 MPa, recovery with ammonia with ~ 0.9 MPa and burning in air with ~ 0.7 MPa). The bearable strength is comparable to those of carbon- and silica-based monolithic species, such as graphene-based cellular monolith[34], nitrogen-rich carbon aerogel monoliths[35] and silica-modified-polymeric monoliths[36]. Such property is very important for actual applications while considering salvageable and stable properties of an adsorbent. Moreover, the BNPMs can adsorb a wide range of oils, revealing excellent adsorption capacities (SI Figure S8). Their remarkable performances for oil-molecule adsorptions can be ascribed to three typically distinct lipophilic performances as reported by Y. Chen, et al[12]: adsorbing on BNPM bubble-wall and macropore surfaces; capillarity effect-assisted filling of microporous structures inside the bubble walls; intercalating into the inter-layer expanded space of a BNPM matrix. Also, the ultra-high SSA and pore volume accelerate the oil adsorption and pore-filling processes, resulting in rapid oil-adsorption behavior. The properties of BNPM adsorbents, especially the unabated recycling stability make them a promising candidate for cleaning oil-polluted water. Due to a fact that the density of the BNPM-1100 (~ 0.18 g/cm^3) is much higher than that for a majority of sponges, like xerogel, aerogel and invented 3D foam adsorbents (with density ranging from 0.0006 to 0.108 g/cm^3)[35, 37-42], it is necessary to evaluate the parameter of volume-based adsorption capacity (VBAC)[35, 37], rather than to rely on simple evaluation by mass-based adsorption capacity. The VBAC of BNPM-1100 for oils was

71% - 98%, indicating that almost the whole volume is available for the oil adsorbance. Such parameter is comparable to those of advanced adsorbents, such as nitrogen-rich/fire-resistance carbon aerogels[35], silica-modified-polymeric monoliths[36], hydrophobicity-modified chitin sponges[37], 3D BN foam scavengers[38], octadecyltrichlorosilane-coated polymerized octadecylsiloxane sponges[39], carbon nanotube/polyurethane sponges[40], cellulose aerogels[41], and high internal phase emulsion xerogels[42] (Table S3 and S4).

Finally, BNPMs were utilized as filtration columns for cleaning water polluted by poisonous dye (RB) or heavy-metal ion (Cd(II)). The strategy is depicted in Figure 8a. The forced pumping enables wastewater to freely flow through the BNPM column (SI Video SV2), evidencing a fast and highly-efficient water purification process. As a result, the cleaned water can be effectively obtained at the other end of the BNPM filter column, for instance, 1000 mL 10^{-5} M RB solution (pH = 7.0) could be completely purified (SI Figure S9). RB removal ability reached ~ 100 % by using permeation column loaded with 50 mg BNPM-1100, with a mean flow rate of 5 mL/min. Furthermore, the breakthrough curve and accumulative adsorbance for RB solution (10^{-4} M at pH = 7.0) through the BNPM-1100 column was investigated, as displayed in Figure 8b. The dynamic investigation indicates that: i) the first 300 mL of RB solution (10^{-4} M) could be fully cleaned (RB removal of ~ 100 %); ii) with increasing liquid permeation volume, the purified capacity of BNPM-1100 shows an exponentially declining trend due to adsorption equilibrium towards a direction of adsorption capacity weakened; iii) approaching over 900 mL achieves the saturated adsorption, and the maximum adsorption capacity of BNPM-1100 reaches up to 554 mg/g. A continuous filtration adsorption process together with desorption cycling was performed by using a more concentrated solution (10^{-3} M) (Figure 8c). In the continuous adsorption-desorption cycles, 25 mL 10^{-3} M RB solution for every filtration can be

completely cleaned into the crystal-pure water (with 100 % RB removal), meanwhile, in every desorption process, ~ 90 % of adsorbed RB can be desorbed by 25 mL ethanol except for the 1st and 10th cycles (SI Figure S10). The introduced desorption process can effectively increase the quantity of completely-cleaned 10^{-3} M RB solution (up to 250 mL) with a total removal capacity rising to ~ 24 g/g. As summarized in SI Table S5, the excellent RB sorption capacity (554 mg/g) of BNPM-1100 is comparable with commercial activated carbon (527 mg/g)[43], but higher than for all possible competitors, including graphenes[44], mesoporous carbon fibers[45], ordered mesoporous carbons[46], kaolinites[47], Fe_3O_4 nanoparticles[48], zeolites[49] and sodium montmorillonites[50]. Such high sorption capacity and fast filtration-sorption behavior are ascribed to a plenty of unsaturated atoms and–OH/-NH_2 groups residing on the walls of micropores and bubble-like holes of BNPM-1100; these are chemically reactive.

Heavy-metal ions, such as Cd(II), can be efficiently adsorbed by BNPM-1100 filtration column as well (Figure 8d). The process displays a similar water-purification trend as that for RB. The Cd(II) ultimate adsorption capacity was 561 mg/g, which is much higher than those of other materials reported, including commercial activated carbons (8 mg/g)[51], mesoporous carbons (406.6 mg/g)[52], multi-walled carbon nanotubes (0.14 mg/g)[53], celluloses (83.6 mg/g)[54], 3D graphene oxide (234.8 mg/g)[55], tetrasulfide-functionalized silica (22.3 mg/g)[56] and zeolites (0.15 mg/g)[57] (SI Table S6), The adsorption capacity of heavy-metal cations is attributed to the ion-exchange mechanism of BNPMs. Zeta-potential measurements reveal that the BNPM-1100 has an overall negative surface charge of about -25.8 mV at pH ≥ 2 (SI Figure S11). Such negative potential is primarily derived from a small amount of –OH/-NH_2 on the BNPM surfaces and numerous unsaturated atomic bonds inside the t-BN structures. The ion-exchange process could be implemented by electrostatic, complex, or hydrogen-bonding interactions between the Cd(II)

and BNPM surfaces and its micro-pore walls. According to the related report[58], the ion-exchanged capacity of BNPM-1100 was determined to be 5.07 mmol/g.

The oil, dye and heavy-metal ion adsorption performances in relation with the hierarchical porous BNPMs are discussed. (1) For the oil adsorption, the first stage, these megapores and macropores provided low-resistant pathways for fast diffusion of oil molecules due to the oleophilic nature of BNPMs surfaces. The second stage, the abundant micropores were filled by oil molecules via capillarity effects, because the micropores inside the BNPMs are mostly hydrophobic and only compatible with hydrophobic oil liquids. The ultra-high surface area and pore volume, and the hierarchical porous structure provide the sufficient spaces for adsorbing oils, making the BNPMs excellent oil adsorbents. (2) For dye and heavy-metal cation ion adsorption, the RB and Cd(II) adsorption behavior mainly depends on the surface effect, such as the properties of the pore walls. A mass of unsaturated atoms along the abundant micropore walls, and a handful of active groups attached on the edges and walls of macropore and megapores, are chemically reactive sites and make a crucial contribution to the RB and Cd(II) adsorptions. Due to the weakly hydrophilic feature of BNPM surfaces, the aqueous solutions of RB and Cd(II) hardly diffuse into the pores by themselves, and must be forced through the pores inside of BNPMs by pumping. Thus an almost complete removal of dye and Cd(II) is implemented successfully by forcing the process through the strong adsorption sites of the hierarchical pore structures.

The reliable recovery, and recycling of BNPMs for application in oil adsorption without damaging their monolithic shape and weakening their adsorption ability (Figure 7), and the continuous adsorption-desorption cycles of RB (Figure 8c), illustrated that the BNPMs are absolutely stable and may be utilized as adsorbents. In addition, the thermal stability of BNPM-

1100 was characterized by TG-DTA (SI Figure S12a), which indicated that BNPM-1100 is quite thermostable in air from room temperature to ~ 960 °C. The samples after adsorption and under recovery after high-temperature ammonia treatments exhibited the same XRD and FTIR features peculiar to the original BNPM-1100 (SI Figure S12b-c), and no morphology change was observed after regeneration (SI Figure S13), this also indicates that the BNPMs are stable when used as an adsorber.

Conclusion

In summary, we successfully prepared the foam-like BN porous monoliths using a facile template-free process involving the solidification of boric acid-dissolved formaldehyde-dicyandiamide resins followed by their high-temperature pyrolysis with ammonia. The obtained BNPMs with the hierarchical pore structures have the highest specific surface area among all BNPM families, and a decent bulk crush strength. They show superb hydrophobicity, high-efficient selective adsorption and excellent overall adsorption capacity for a diverse range of oils. In addition the material also exhibits the reliable recovery and recycling giving no damage to its monolithic shape, and no weakening to its adsorption ability over many cycles. Lastly, the BNPM filtration columns were shown to have outstanding filtration adsorption of RB dyes and heavy-metal cations Cd(II) under a rapid forced pumping process, realizing a high-efficient cleaning process of contaminated water. These results indicate that the fabricated BNPMs have a great potential for high-end applications in water purification and treatment.

Acknowledgements

The authors thank the financial support from the World Premier International (WPI) Center for Materials Nanoarchitectonics (MANA) of the National Institute for Materials Science (NIMS),

Grant No. BB005, and National Natural Science Foundation of China (No. 51372066). The authors acknowledge the help of Kun Chang (NIMS) providing chemical reagent (Cadmium Chloride) to them.

References

1. T. Barroso, T. Casimiro, A. M. Ferraria, F. Mattioli, A. Aguiar-Ricardo and A. C. A. Roque, *Adv. Funct. Mater.*, 2014, **24**, 4528-4541.
2. G. P. Hao, W. C. Li, D. Qian and A. H. Lu, *Adv. Mater.*, 2010, **22**, 853-857.
3. G. P. Hao, W. C. Li, D. Qian, G. H. Wang, W. P. Zhang, T. Zhang, A. Q. Wang, F. Schuth, H. J. Bongard and A. H. Lu, *J. Am. Chem. Soc.*, 2011, **133**, 11378-11388.
4. Y. Wang, S. Tao and Y. An, *J. Mater. Chem. A*, 2013, **1**, 1701-1708.
5. A. Inayat, B. Reinhardt, H. Uhlig, W. D. Einicke and D. Enke, *Chem. Soc. Rev.*, 2013, **42**, 3753-3764.
6. C. Moreno-Castilla and A. F. Pérez-Cadenas, *Materials*, 2010, **3**, 1203-1227.
7. D. Golberg, Y. Bando, Y. Huang, T. Terao, M. Mitome, C. Tang and C. Zhi, *ACS NANO*, 2010, **4**, 2979-2993.
8. R. T. Paine and C. K. Narula, *Chem. Rev.*, 1990, **90**, 73-91.
9. S. Bernard and P. Miele, *New J. Chem.*, 2014, **38**, 1923.
10. P. Dibandjo, L. Bois, C. Estournes, B. Durand and P. Miele, *Microporous Mesoporous Mater.*, 2008, **111**, 643-648.
11. J. G. Alauzun, S. Ungureanu, N. Brun, S. Bernard, P. Miele, R. Backov and C. Sanchez, *J. Mater. Chem.*, 2011, **21**, 14025.
12. W. Lei, D. Portehault, D. Liu, S. Qin and Y. Chen, *Nat. Commun.*, 2013, **4**, 1777.
13. J. Li, J. Lin, X. Xu, X. Zhang, Y. Xue, J. Mi, Z. Mo, Y. Fan, L. Hu, X. Yang, J. Zhang, F. Meng, S. Yuan and C. Tang, *Nanotechnology*, 2013, **24**, 155603.
14. J. Li, X. Xiao, X. Xu, J. Lin, Y. Huang, Y. Xue, P. Jin, J. Zou and C. Tang, *Sci. Rep.*, 2013, **3**, 3208.
15. G. Lian, X. Zhang, S. Zhang, D. Liu, D. Cui and Q. Wang, *Ener. Environ. Sci.*, 2012, **5**, 7072-7080.
16. F. Liu, J. Yu, X. Ji and M. Qian, *ACS Appl. Mater. Inter.*, 2015, **7**, 1824-1832.
17. Q. Weng, X. Wang, C. Zhi, Y. Bando and D. Golberg, *ACS NANO*, 2013, **7**, 1558-1565.
18. S. Zhang, G. Lian, H. Si, J. Wang, X. Zhang, Q. Wang and D. Cui, *J. Mater. Chem. A*, 2013, **1**, 5105-5112.
19. Y. Xue, Q. Liu, G. He, K. Xu, L. Jiang, X. Hu and J. Hu, *Nanoscale. Res. Lett.*, 2013, **8**, 1-7.
20. J. Thomas, N. E. Weston and T. E. O'connor, *J. Am. Chem. Soc.*, 1962, **84**, 4619-4622.
21. J. Zhang, Z. Tan, S. Meng, S. Li and L. Zhang, *Thermochim. Acta*, 1997, **307**, 11-15.
22. Q. Weng, X. Wang, Y. Bando and D. Golberg, *Adv. Energy. Mater.*, 2014, **4**, 1-8.
23. X. Wang, C. Zhi, L. Li, H. Zeng, C. Li, M. Mitome, D. Golberg and Y. Bando, *Adv. Mater.*, 2011, **23**, 4072-4076.
24. S. Schlienger, J. Alauzun, F. Michaux, L. Vidal, J. Parmentier, C. Gervais, F. Babonneau,

S. Bernard, P. Miele and J. B. Parra, *Chem. Mater.*, 2012, **24**, 88-96.
25. M. A. Parent and J. B. Moffat, *Langmuir*, 1995, **11**, 4474-4479.
26. J. Landers, G. Y. Gor and A. V. Neimark, *Colloids Surf. Physicochem. Eng. Aspects*, 2013, **437**, 3-32.
27. A. V. Neimark, Y. Lin, P. I. Ravikovitch and M. Thommes, *Carbon*, 2009, **47**, 1617-1628.
28. Q. Weng, Y. Ide, X. Wang, X. Wang, C. Zhang, X. Jiang, Y. Xue, P. Dai, K. Komaguchi, Y. Bando and D. Golberg, *Nano Energy*, 2015, **16**, 19-27.
29. M. H. Khan, Z. Huang, F. Xiao, G. Casillas, Z. Chen, P. J. Molino and H. K. Liu, *Sci. Rep.*, 2015, **5**, 7743.
30. Z. Liu, Y. Gong, W. Zhou, L. Ma, J. Yu, J. C. Idrobo, J. Jung, A. H. MacDonald, R. Vajtai, J. Lou and P. M. Ajayan, *Nat. Commun.*, 2013, **4**, 2541.
31. L. Song, L. Ci, H. Lu, P. B. Sorokin, C. Jin, J. Ni, A. G. Kvashnin, D. G. Kvashnin, J. Lou, B. I. Yakobson and P. M. Ajayan, *Nano Lett.*, 2010, **10**, 3209-3215.
32. F. Müller, S. Hüfner, H. Sachdev, S. Gsell and M. Schreck, *Phys. Rev. B*, 2010, **82**.
33. T. Sainsbury, T. Ikuno, D. Okawa, D. Pacile, J. M. J. Frechet and A. Zettl, *J. Phys. Chem. C*, 2007, **111**, 12992-12999.
34. L. Liu, J. Z. Liu, S. L. Y. Chang, Y. Z. Wu and D. Li. *Nat. Commun.*, 2012, **3**, 1241.
35. Y. Yang, Z. Tong, T. Ngai and C. Wang, *ACS Appl. Mater. Inter.*, 2014, **6**, 6351-6360.
36. X. Chen, L. Liu, k. Liu, Q. Miao and Y. Fang, *J. Mater. Chem. A*, 2014, **2**, 10081-10089.
37. B. Duan, H. Gao, M. He and L. Zhang, *ACS Appl. Mater. Inter.*, 2014, **6**, 19933-19942.
38. H. Zhao, X. Song and H. Zeng, *NPG Asia Mater.*, 2015, **7**, e168.
39. Q. Ke, Y. Jin, P. Jiang and J. Yu, *Langmuir*, 2014, **30**, 13137-13142.
40. H. Wang, E. Wang, Z. Liu, D. Gao, R. Yuan, L. Sun and Y. Zhu, *J. Mater. Chem. A*, 2015, **3**, 266-273.
41. S. T. Nguyen, J. Feng, N. T. Le, A. T. T. Le, N. Hoang, V. B. C. Tan and H. M. Duong, *Ind. Eng. Chem. Res.*, 2013, **52**, 18386-18391.
42. Y. Wu, T. Zhang, Z. Xu and Q. Guo, *J. Mater. Chem. A*, 2015, **3**, 1906-1909.
43. F. Hayeeye, M. Sattar, S. Tekasakul and O. Sirichote, *Songklanakarin J. Sci. Tech.*, 2014, **36**, 177-187.
44. K. Liua, H. Li, Y. Wang, X. Gou, Y. Duan and *Colloids Surf. Physicochem. Eng. Aspects*, 2015, **477**, 35-41.
45. Y. Dong, H. Lin, Q. Jin, L. Li, D. Wang, D. Zhou and F. Qu, *J. Mater. Chem. A*, 2013, **1**, 7391-7398.
46. X. Zhuang, Y. Wan, C. Feng, Y. Shen and D. Zhao, *Chem. Mater.*, 2009, **21**, 706-716.
47. T. A. Khan, S. Dahiya and I. Ali, *Appl. Clay Sci.*, 2012, **69**, 58-66.
48. L. Peng, P. Qin, M. Lei, Q. Zeng, H. Song, J. Yang, J. Shao, B. Liao and J. Gu, *J. Hazard. Mater.*, 2012, **209-210**, 193-198.
49. F. Jafari-zare and A. Habibi-yangjeh, *Chin. J. Chem* . 2010, **28**, 349-356.
50. P. P. Selvam, S. Preethi, P. Basakaralingam, N. Thinakaran, A. Sivasamy and S. Sivanesan, *J. Hazard. Mater.*, 2008, **155**, 39-44.
51. S. Hydari, H. Sharififard, M. Nabavinia and M. r. Parvizi, *Chem. Eng. J.*, 2012, **193-194**, 276-282.
52. G. Zeng, Y. Liu, L. Tang, G. Yang, Y. Pang, Y. Zhang, Y. Zhou, Z. Li, M. Li, M. Lai, X. He and Y. He, *Chem. Eng. J.*, 2015, **259**, 153-160.
53. M. Abdel Salam, *Int. J. Environ. Sci. Te.*, 2013, **10**, 677-688.
54. J. Liu, T. Xie, C. Deng, K. Du, N. Zhang, J. Yu, Y. Zou and Y. Zhang, *Sep. Sci. Technol.*,

2014, **49**, 1096-1103.
55. S. Wu, K. Zhang, X. Wang, Y. Jia, B. Sun, T. Luo, F. Meng, Z. Jin, D. Lin, W. Shen, L. Kong and J. Liu, *Chem. Eng. J.*, 2015, **262**, 1292-1302.
56. H. Fan, J. Wu, X. Fan, D. Zhang, Z. Su, F. Yan and T. Sun, *Chem. Eng. J.*, 2012, **198-199**, 355-363.
57. L. Remenarova, M. Pipiska, E. Florkova, M. Hornik, M. Rozloznik and J. Augustin, *Clean Technol. Envir.*, 2014, **16**, 1551-1564.
58. H.-W. Liang, X. Cao, W.-J. Zhang, H.-T. Lin, F. Zhou, L.-F. Chen and S.-H. Yu, *Adv. Funct. Mater.*, 2011, **21**, 3851-3858.

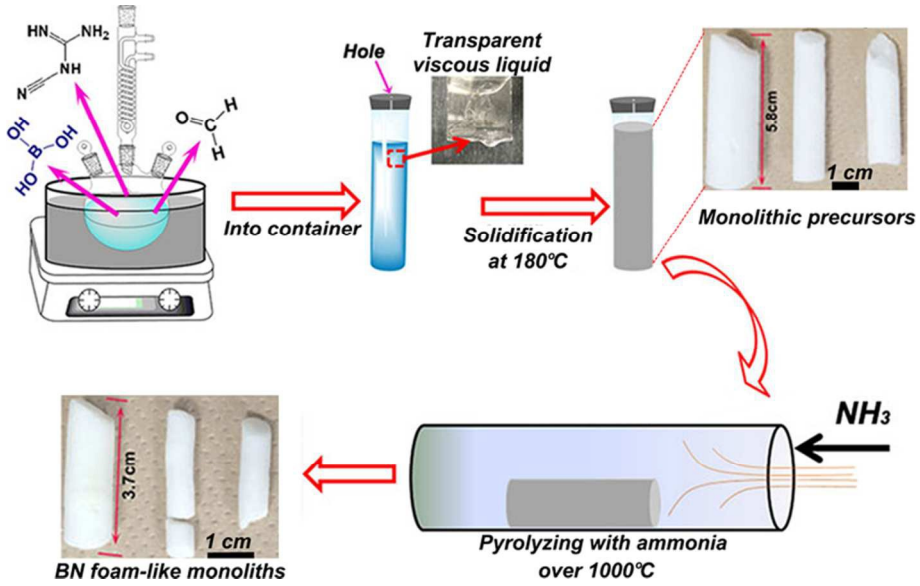

Figure 1. Schematic diagram of the BN foam-like monoliths synthesis.

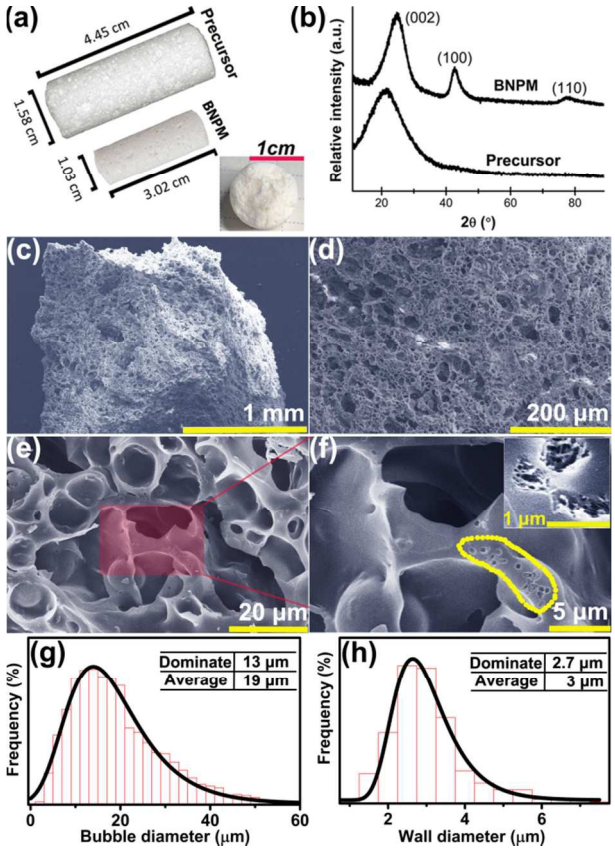

Figure 2 a) Photograph of a precursor monolith and BNPM, Inset: cross-section of columnar BNPM. b) Representative XRD patterns of the precursor monolith and BNPM-1100 °C. c- f) Representative SEM images of BNPM. Yellow frame of f) showing the macropores on the bubble wall. The inset in f) shows an enlarged part of the small yellow frame, indicating macropores with diameter of ~ 1 μm. g-h) A size distribution histograms of bubble diameters and bubble wall thickness, and their Gaussian fit, showing the dominant values of 13 μm and 2.7 μm, and average values of 19 μm and 3 μm.

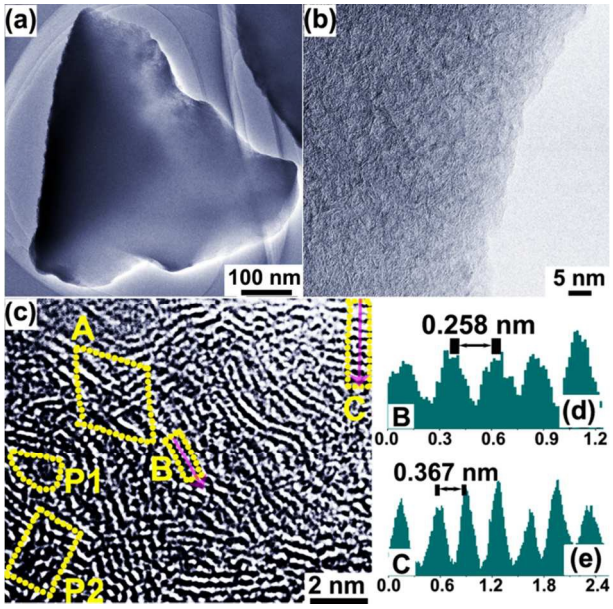

Figure 3 a-c) TEM and HRTEM images taken at the edge of BNPM bulk. Dislocation positions, and possible P1 and P2 pore types are marked with yellow frames. A frame showing possible unparallel and crossed layer-structure models. d-e) TEM contrast intensity profile recorded along the red arrows of B and C yellow frames in c).

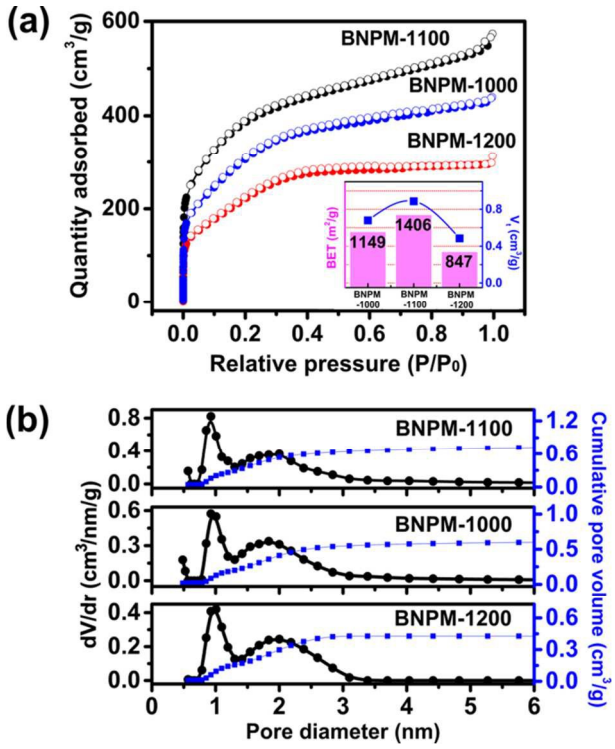

Figure 4 a) Nitrogen adsorption-desorption isotherms of BNPM pyrolyzed at 1000, 1100 and 1200 °C. Inset in a) showing summary of the BET specific surface areas and total pore volumes (V_t) of as-measured samples. b) The pore size distribution and cumulative pore volume plots of BNPM using the quenched solid state functional theory.

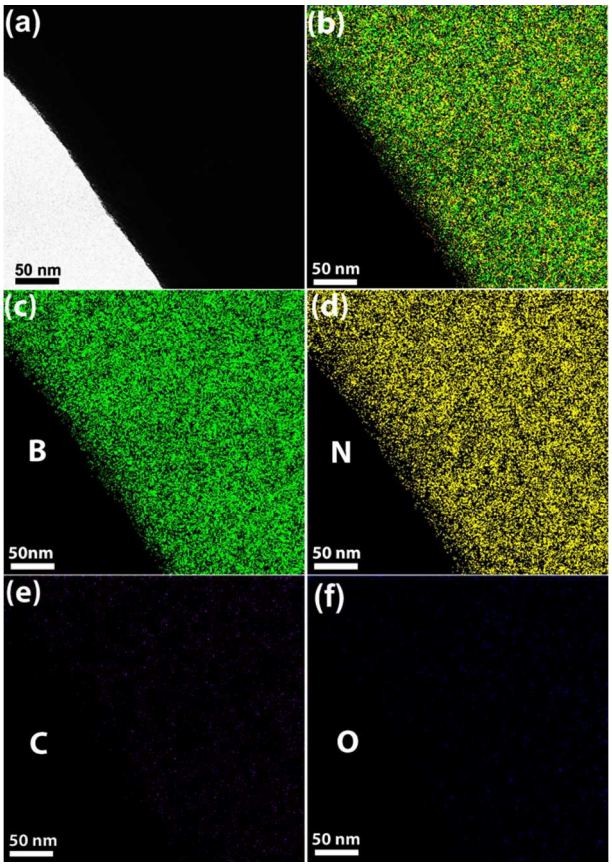

Figure 5 a) Zero-loss TEM image of BNPM bulk edge. b) An overlay of B, N, C and O elemental mappings. c-f) The individual spatially-resolved distribution of B, N, C and O species, respectively.

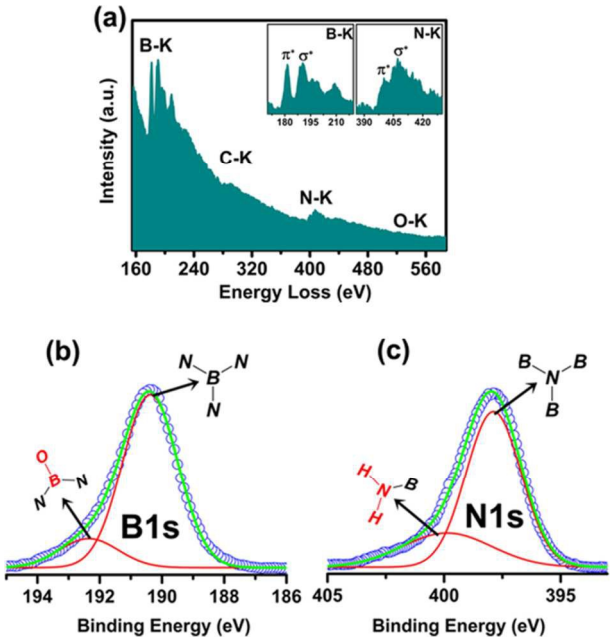

Figure 6. a) EELS of a BNPM-1100 sample. b) The B1s XPS spectrum of BNPM-1100 was deconvoluted into two chemical states of B atoms, namely, B-OH (192.4 eV) and N-B-N (190.3 eV). c) Its corresponding N1s XPS spectum was deconvoluted into H–N-H (399.8 eV) and B-N-B (398.0 eV) chemical states of N atoms.

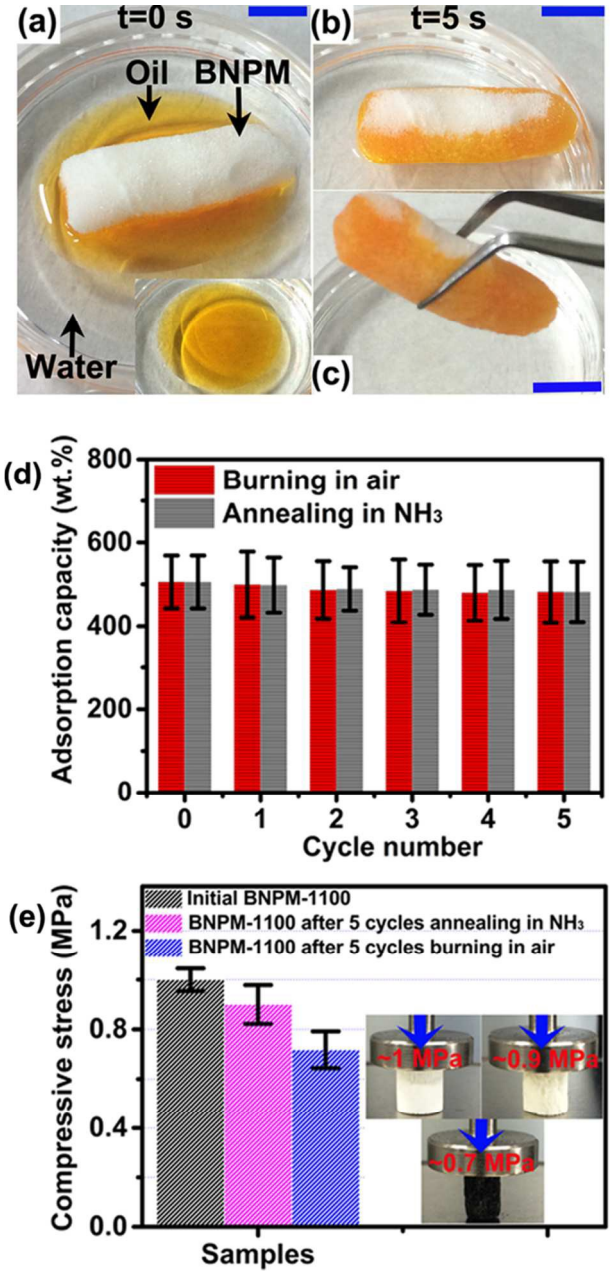

Figure 7 a-b) Photos on adsorption process of a salad oil by using BNPM-1100 within 5 s. c) After adsorption was completed, the bulk BNPM-1100 could be conveniently clipped out from water using tweezers. d) Recyclability of BNPM for oil adsorption after burning in air and annealing in NH_3 atmosphere at 900 °C. g) The bulk crush strengths of the samples. Insets show the photographs of corresponding samples under compressive tests.

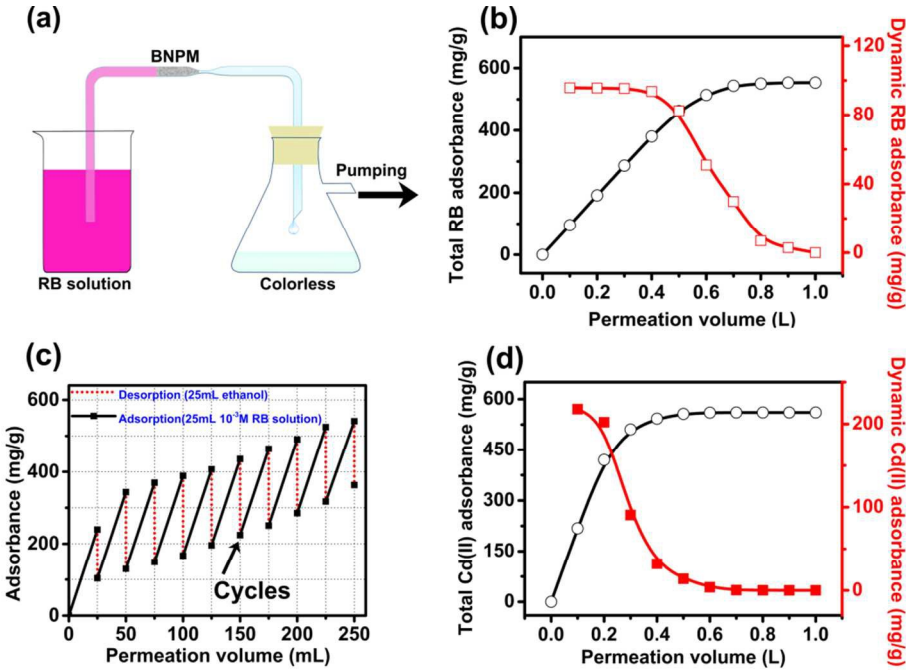

Figure 8 a) The schematic diagram of the designed filtration adsorption test. b) Breakthrough curve and accumulative adsorbance for passage of RB solution through the BNPM-1100 permeation column with a feed concentration of 10^{-4} M at pH=7.0. c) Adsorption and desorption of RB through pumping filtration, using 25 mL 10^{-3} M RB feed solution at pH=7.0 for every adsorption cycle followed by pumping filtration 25 mL ethanol per desorption cycle with 50 mg BNPM-1100. d) Breakthrough curve and accumulative adsorbance of Cd(II) ions using pumping filtration with 50 mg BNPM-1100 permeation column with 10^{-3} M $CdCl_2$ aqueous solution at pH=7.0, with a mean flow rate of ~ 3 mL/min.

Table of content (TOC)

New boron nitride porous monoliths with high-efficiency and excellent adsorption applications were successfully fabricated by a bran-new and template-free method.